

ULTRA-COMPACT EMBEDDED CLUSTERS IN THE GALACTIC PLANE

Michael J. Alexander¹ and Henry A. Kobulnicky¹

ABSTRACT

We have identified a previously unrecognized population of very compact, embedded low-mass Galactic stellar clusters. These tight ($r \approx 0.14$ pc) groupings appear as bright singular objects at the few arcsec resolution of the *Spitzer Space Telescope* at 8 and 24 μm but become resolved in the sub-arcsecond UKIDSS images. They average six stars per cluster surrounded by diffuse infrared emission and coincide with 100 – 300 M_{\odot} clumps of molecular material within a larger molecular cloud. The magnitudes of the brightest stars are consistent with mid-to early-B stars anchoring $\sim 80 M_{\odot}$ star clusters. Their evolutionary descendants are likely to be Herbig Ae/Be pre-main sequence clusters. These ultra-compact embedded clusters (UCECs) may fill part of the low-mass void in the embedded cluster mass function. We provide an initial catalog of 18 UCECs drawn from infrared Galactic Plane surveys.

Subject headings: open clusters and associations: general — stars: pre-main sequence — infrared: stars

1. Introduction

Most, if not all, stars are born in stellar clusters. It has been estimated that 96% of massive OB ($>8 M_{\odot}$) stars are associated with clusters (de Wit et al. 2005). For nearby ($\lesssim 2$ kpc) embedded star clusters, Lada & Lada (2003) found a flat mass distribution function, implying a power law ($\alpha = -2$) distribution by number for young clusters. Their relation exhibits a sharp turnover for clusters with total stellar masses less than $\sim 50 M_{\odot}$ and suggests that $>90\%$ of all stars form in clusters more massive than this lower limit. Gutermuth et al. (2009) surveyed 36 star clusters in young star-forming regions (SFRs), mostly within 1 kpc of the sun, and found an average of 26 members per cluster with mean radii of 0.39 pc. These clusters are quite young, as evidenced by their high incidence of young stellar objects

¹Department of Physics and Astronomy, University of Wyoming, Laramie, WY 82071, USA

(YSOs). Despite recent advances and observations, the census of the smallest embedded clusters is still incomplete owing to the limited depth and angular resolution of large scale infrared (IR) surveys.

During a study of SFRs in the Galactic Plane (Alexander et al. 2012), we serendipitously identified two compact stellar clusters. These objects have pointlike or marginally resolved morphologies in the few arcsecond resolution mid-IR *Spitzer Space Telescope* images at [8.0] and [24] μm , but are resolved in the sub-arcsecond *JHK* images from the United Kingdom Infrared Deep Sky Survey (UKIDSS; Lucas et al. 2008). The mid-IR images are typically dominated by a single bright object that exhibits a steeply rising spectral energy distribution (SED) through the mid-IR. The putative clusters are often found within infrared dark clouds (IRDCs) surrounded by nebulosities tracing the hot dust, reflection nebulosity, and PAH emission characteristic of young embedded clusters.

Using brightness and color criteria derived from the prototype sources, we searched for similar objects in the Galactic Legacy Infrared MidPlane Survey Extraordinaire (GLIMPSE; Benjamin et al. 2003) Point Source Catalogs (PSCs) as well as a subsample of massive YSO (MYSO) candidates from the *MidCourse Space Experiment (MSX)* Red MSX Source (RMS) catalog (Urquhart et al. 2011). The search yielded additional candidates, and we present an initial (incomplete) sample of 18 ultra-compact embedded clusters (UCECs) and their properties.

2. Identification of Candidate Clusters

We used the mid-IR magnitudes of the prototype clusters to define two criteria to search for additional candidate clusters in the GLIMPSE PSCs. We required that sources have a red IR color¹ ($K_S - [3.6] > 2$) and a bright (< 5 mag.) GLIMPSE detection. Although the second criterion allows for any IRAC band, it is nearly always satisfied by [8.0] as the other bands saturate at fainter magnitudes. The search was limited to the GLIMPSE I area that overlaps with UKIDSS (≈ 96 sq. deg. between $\ell = 15^\circ - 66^\circ$) to ensure the availability of high-resolution imaging. These criteria pick out 391 candidate clusters for which we examined UKIDSS images and tentively identified three types of objects: evolved stars, single YSOs, and potential clusters. We eliminated objects that appeared single and isolated, lacking apparent extended structures; these constituted the majority of the initial list and are most likely field giants or AGB stars. We retained six objects that exhibited multiple red stars

¹GLIMPSE PSCs include *JHK_S* photometry from the Two Micron All Sky Survey (2MASS, Skrutskie et al. 2006).

with rising SEDs; these types of objects were invariably accompanied by an extended near-IR nebosity, most prominently at K band.

Literature searches on color-selected clusters revealed that several were identified previously as candidate MYSOs. Therefore, we expanded our search to include MYSO candidates from Table 3 of Urquhart et al. (2011), which have estimated distances. The UKIDSS images revealed that some of the MYSO candidates appear to be small stellar clusters. The classification is ambiguous in some cases because of the high levels of diffuse emission associated with the objects. We found 12 objects that are candidate compact stellar clusters.

Table 1 lists the 18 most compelling UCEC candidates. Column 1 is the ID number and columns 2 and 3 are Galactic longitude and latitude. Column 4 is the angular radius, r_c , estimated by-eye to include sources within the IR nebosity. Column 5 is number of stars per cluster, N_* , with a membership probability greater than 75% after background subtraction (discussed below). Column 6 is the LSR velocity of the peak ^{13}CO emission from the Galactic Ring Survey (Jackson et al. 2006), and column 7 is the near kinematic distance derived from the velocity and a rotation curve (Clemens 1985). Column 8 is the gas mass derived from the distance in column 7 and the 1.1 mm flux from the Bolocam Galactic Plane Survey (BGPS) Catalog using Equation 2 from Rosolowsky et al. (2010), unless otherwise specified. Column 9 gives the physical radius, R_p , column 10 is the associated MSX ID (Urquhart et al. 2011), if applicable, and column 11 specifies if there is evidence for an associated compact HII region from the Multi-Array Galactic Plane Imaging Survey (MAGPIS, Helfand et al. 2006) 6 or 20 cm maps.

3. Ultra-compact Embedded Clusters

3.1. General Properties

Figure 1 is a three-color ($[4.5]$, $[8.0]$, and $[24]$) image of four UCECs. Blue circles mark the locations of the UCECs and have radii given in Table 1. The $1'$ yellow bar illustrates the linear size scale in pc at the adopted distance, and black contours outline BGPS 1.1 mm emission. UCEC #13 (lower-left) falls outside the BGPS coverage so no contours are shown, however, IRDCs are apparent within the region. Most of the UCECs in Table 1 have associated IRDCs indicating that these regions are active, or future, SFRs and likely lie at the near kinematic distance. The IRDCs connected with the clusters contain a median gas mass of $141 M_\odot$; the millimeter continuum maps indicate that they are generally part of larger molecular clouds.

The prototype UCECs are $\sim 5 - 11''$ in radius and appear pointlike at $[8.0]$ and $[24]$,

while the [3.6] and [4.5] images may partially resolve the clusters into 2 – 4 highly blended sources. The average IRAC magnitudes for the brightest point source in an individual UCEC are 7.9, 7.3, 5.7, and 4.9 for [3.6], [4.5], [5.8], and [8.0], quite close to the saturation limits. The magnitudes demonstrate a rising SED typical of YSOs and indicate the extreme youth and/or embedded nature of these objects. Although the cluster radius is large compared to the 1".2 pixel size of IRAC, the combination of source brightness and high source density makes it difficult or impossible to resolve individual stars, and it is not obvious that the sources contain compact clusters.

We estimated field star contamination by comparing H vs. $H - K$ cluster color-magnitude diagrams (CMDs) with field CMDs using UKIDSS DR7 photometry². The cluster radius, r_c , defined the target area, and an annulus from r_c to 33" was the field area. The field should be large enough to provide good statistics yet small enough to represent the local field population and extinction. The cluster and field CMDs were divided into bins and compared, yielding the membership probability, $P = (N_C - A \times N_F) / N_C$, where N_C is the number of target stars a given bin, N_F is the field star count, and A is target-to-field area ratio. We used 729 bin size and center combinations to mitigate biases caused by any particular binning strategy. This is similar to the procedure used by Maia et al. (2010), except that high extinction towards UCECs reduces J-band source counts so we are limited to H- and K-band. This technique estimates where a cluster lies in color-magnitude space but cannot tell if an individual star is a member because stars are selected statistically. A true assignment of cluster membership generally requires stellar spectra to assign a spectral type and distance.

Figure 2 shows zoomed three-color UKIDSS JHK (blue, green, and red) images of the four UCECs, as in Figure 1, where the yellow bar is now 30". The cluster nature of these sources is more pronounced at sub-arcsecond resolution, but there is still some source blending. The UCECs exhibit structured diffuse emission, likely arising from hot dust and/or reflection nebulosity. These sources span distances from 2 – 7 kpc, but have similar physical sizes.

3.2. UCEC #5

UCEC #5 (Figure 2, upper-left) shows the highest field star density, consistent with its large distance of 7.3 kpc. Figure 3 (upper-left) is an H vs ($H - K$) CMD for #5 showing cluster members (>75% probability) as pluses and field stars as grey dots. The solid and

²<http://surveys.roe.ac.uk/wsa/>

dotted lines are a zero-age main sequence (ZAMS) isochrone (Marigo et al. 2008) and a 0.5 Myr pre-main sequence isochrone (PMS, Siess et al. 2000), respectively. Both have been placed at the estimated cluster distance (7.3 kpc) and extincted according to the reddening vector (Cardelli et al. 1989). The diamond, circle, and asterisk on the MS isochrone mark the location of an A0, B2, and O9 star, respectively. The molecular cloud associated with #5 has a radial velocity $V_{LSR} = 103.9 \text{ km s}^{-1}$ and lies near the tangent point in this direction, making the distance unambiguous. The extinction value was estimated by-eye to match the locus of putative cluster members. The spread in $H - K$ is likely caused by strong differential reddening within the cluster, so cluster members are not expected to lie along any single isochrone. The two brightest sources may be O stars, if they are single, while the rest fall in the early-B range.

UCEC #5 protrudes from the edge of a bright-rimmed cloud (Figure 1, upper left) likely formed by a known HII region (Lockman 1989). The rim of PAH and molecular material is traced by the 1.1 mm continuum contours and may indicate the presence of a swept-up shell of material making the cluster a candidate for triggered star formation (SF). The millimeter emission suggests a total molecular gas mass of $5400 M_{\odot}$ for the entire clump. However, the emission does not peak over the cluster, so we estimate an upper limit of $130 M_{\odot}$ for the gas mass within a $9''$ radius of the UCEC. The cluster itself does not exhibit a peak in either the 6 or 20 cm maps from MAGPIS ($2''$ and $6''$ beam FWHM, respectively), but diffuse radio continuum from the main HII region precludes an accurate upper limit.

3.3. UCEC #8

UCEC #8 was the first UCEC identified and appears in the upper-right panel of the figures. Figure 1 shows the UCEC sandwiched between an IR-bright bubble (N74, Churchwell et al. 2006) and the edge of an IRDC. Jackson et al. (2006) place the IRDC at the near distance of 2.7 kpc, which we adopt for the UCEC. The upper-right panel of Figure 3 shows the cleaned CMD, with symbols as before. The eight sources within this region display a similar color and suggests that they occupy the same volume. Most of the sources are again consistent with early-B stars, taking into account differential reddening. The 1.2 mm maps presented by Rathborne et al. (2006) have higher resolution ($11''$ FWHM) than the BGPS ($33''$ FWHM), so we adopt their gas mass estimates of $1792 M_{\odot}$ for the entire IRDC and $73 M_{\odot}$ for the peak coincident with the UCEC.

3.4. UCEC #13

Figure 1 (lower-left) shows the extreme mid-IR brightness of UCEC #13, as well as nearby IRDCs. Figure 2 reveals the cluster nature of the object and shows many bright sources embedded in diffuse emission. The CMD for this cluster (Figure 3, lower-left panel) shows six sources consistent with B star magnitudes at approximately $A_V = 15$ mag. UCEC #13 falls outside the BGPS coverage but has a detection from the James Clerk Maxwell Telescope (JCMT) at $450\ \mu\text{m}$ (Di Francesco et al. 2008). We use Equation 9 from Rosolowsky et al. (2010) to calculate the total gas mass of the cloud, adopting 3.0 kpc for the distance, $6.7\ \text{cm}^2\ \text{g}^{-1}$ for the dust grain opacity (Ossenkopf & Henning 1994), and a dust-to-gas ratio of 0.01. This yields a total mass for the region of $217\ M_\odot$.

3.5. UCEC #16

UCEC #16 (Figure 1, lower-right) is situated at the center of an IRDC complex. The bright core is saturated in the mid-IR images, and several bright point sources, likely YSOs, are scattered throughout the IRDC. Figure 2 shows that all sources within the cluster radius are extremely red. This is evident in the CMD (Figure 3) which shows all five of the stars have $(H - K) > 2$ and implies $A_V > 30$. At the estimated distance and reddening, they are consistent with B stars. This region lies at a distance of 1.8 kpc and has a total gas mass of $124\ M_\odot$ (Rathborne et al. 2006).

4. Discussion

Our initial search shows that young, embedded compact clusters can be selected by an IR color and magnitude cut with follow-up visual inspection. Undoubtedly, there are additional compact clusters that remain unidentified because of very high extinction, large field star densities, extreme compactness, or incompleteness stemming from high diffuse background levels. Our analysis revealed that all 12 of the UCECs from the MYSO sample were missing either a 2MASS K_S or $[8.0]$ catalog entry. The missing detection at K_S is probably from source blending, while at $[8.0]$ saturation likely kept the object out of the point source catalogs. Therefore, this color selection technique is limited to sources faint enough to be unsaturated in GLIMPSE. If we were to relax the selection criteria to include fainter sources with $[8.0] = 5\text{--}6$ mag, the number of selected objects increases to more than a thousand. These could include even lower-mass clusters and those too faint to be included in the MSX catalog, but visual classification of such a large sample is beyond the scope of

this work.

Sub-arcsecond mid-IR imaging was performed on 14 MYSO candidates at $24.5\ \mu\text{m}$ (de Wit et al. 2009) and on 346 MYSOs at $10.3\ \mu\text{m}$ (Mottram et al. 2007). These studies found that approximately 20 – 25% of MYSO candidates have multiple detections and/or extended diffuse emission. These wavelengths primarily detect stars with strong IR excesses rather than stellar photospheres and may miss sources that lack or have only a weak excess. However, their results are consistent with a portion of MYSO candidates being compact stellar clusters.

Only four of 18 UCECs have possible radio detections. UCEC #11 was detected at 3.6 and 1.3 cm by Sánchez-Monge et al. (2008) and they estimate a spectral type of B2 – B3 for the exciting source. Three others (#4, #5, and #6) appear to be associated with faint 20 cm emission from the MAGPIS survey (Helfand et al. 2006), however they do not appear in the MAGPIS point source catalog (White et al. 2005). The estimated completeness limit at 20 cm is 14 mJy, which is sensitive enough to detect an O9.5V at 10 kpc based on the Lyman continuum flux (Martins et al. 2005). This indicates that the most massive star(s) within the majority the UCECs is an early-B star producing relatively few Lyman continuum photons, consistent with the inferences drawn from the CMDs in Figure 3. Another possibility is that the stars earlier than B0 are so young that they have not yet formed a detectable HII region (Urquhart et al. 2011). In some cases a single, bright source appears to dominate the UCECs and may in fact be a MYSO, but in others the IR flux is more evenly distributed among cluster members, in which case the most massive star may be an early- to mid-B star.

Testi et al. (1997) identified small clusters of PMS stars around Herbig Ae/Be stars. These clusters have radii of about 0.2 pc, typically contain 4 – 12 stars, and <few Myr old. In these clusters the maximum stellar mass is correlated with the K band source counts. Field-star-subtracted source counts (6–8 stars) from Figure 3 are roughly consistent with those found in Herbig Be PMS clusters (2–16) (Testi et al. 1999). It is likely that UCECs suffer a higher level of extinction owing to their highly embedded nature and, as a result, source counts within UCECs may be underestimated compared to more exposed and evolved Herbig Ae/Be clusters. This evidence suggests that UCECs represent a younger, more heavily embedded phase destined to evolve into Herbig Ae/Be clusters after a few Myr.

Weidner et al. (2010) found a correlation between the most-massive cluster member (m_{max}) and the total cluster mass (M_{ecl}) that cannot be explained by a random sampling of the IMF. The m_{max} - M_{ecl} relation is incomplete below $100\ M_{\odot}$ (Weidner et al. 2010), but is supported by later investigations (Kirk & Myers 2011). An accurate determination of M_{ecl} depends on cluster age because of the increasing probability of losing cluster members over time (Boily & Kroupa 2003). UCECs are ideal objects for further probing the m_{max} - M_{ecl}

relation because they are likely to have $M_{ecl} < 100 M_{\odot}$ and young enough to have not lost a significant number of cluster stars.

Figure 3 indicates that m_{max} is near an $\sim 8 M_{\odot}$ B2V star, which implies $M_{ecl} \sim 80 M_{\odot}$, while an O9V star ($\sim 20 M_{\odot}$) and a B8V ($\sim 4 M_{\odot}$) would have M_{ecl} of 251 and 26 M_{\odot} , respectively (Weidner et al. 2010). If UCECs are 80 M_{\odot} clusters the SF efficiency, $SFE = M_*/(M_* + M_{gas})$ would be 0.52, 0.27, and 0.39 for #8, #13, and #16, respectively, while the median gas mass of the entire sample (141 M_{\odot}) produces a SFE of 0.36. These SFE values are slightly higher, though still consistent, with studies of other Galactic clusters and SFRs (Lada & Lada 2003; Alves et al. 2007). The CMDs in Figure 3 show that the clusters may contain more than one early-B star, which would increase the implied number of unseen low-mass stars for a standard IMF. These sources are absent either because they fall below the UKIDSS detection limit or the IMF is truncated in these types of objects.

After stars form within a cluster, they immediately begin to expel the surrounding ISM. The rapid expulsion of gas alters the cluster’s potential well and may cause clusters to dissolve (Boily & Kroupa 2003). Lada & Lada (2003) estimate up to 95% of embedded clusters will disperse in under 5 – 10 Myr, and those that do survive longer typically have masses over 500 M_{\odot} . This puts an upper limit on the lifetime of UCECs ($<$ a few Myr) and suggests that they will quickly disperse. Such clusters, in any case, would be difficult to identify after a few Myr once the large IR luminosity arising in circumstellar and intracluster dust diminishes.

Jackson et al. (2010) suggest that IRDCs are the precursors to massive stars and star clusters. The presence of UCECs embedded within IRDCs supports this hypothesis. After several Myr, it is likely that the IRDC will have dissipated and SF ceased. Small clusters, including UCECs, will be disrupted and may appear as a single loose cluster or stellar association of a few hundred solar masses. Thus, large stellar associations may be comprised of the distributed remnants of many smaller clusters born out of the same IRDC. The gas-free merger of small clusters may explain why the m_{max} - M_{ecl} relation differs from random IMF sampling (for clusters $> 100 M_{\odot}$) by limiting accretion and growth of the most massive members, except in the most massive molecular clouds (Weidner et al. 2010).

UCECs may represent an unrecognized but significant population of low-mass stellar clusters destined to quickly disperse into the Galactic stellar field. In large enough numbers, these types of objects may be numerous enough to steepen the low-mass end of the embedded cluster mass function.

We wish to thank our anonymous referee for many helpful comments. We also thank Charles Kerton and Ed Churchwell for their suggestions. MJA is supported by NASA GSRP

fellowship NNX 10-AM10H. HAK is supported by NASA grant ADAP-NNX10AD55G.

REFERENCES

- Aguirre, J. E., Ginsburg, A. G., Dunham, M. K., et al. 2011, *ApJS*, 192, 4
- Alexander, M. J., et al. 2012, in prep.
- Alves, J., Lombardi, M., & Lada, C. J. 2007, *A&A*, 462, L17
- Benjamin, R. A., Churchwell, E., Babler, B. L., et al. 2003, *PASP*, 115, 953
- Billot, N., Noriega-Crespo, A., Carey, S., et al. 2010, *ApJ*, 712, 797
- Boily, C. M., & Kroupa, P. 2003, *MNRAS*, 338, 665
- Cardelli, J. A., Clayton, G. C., & Mathis, J. S. 1989, *ApJ*, 345, 245
- Churchwell, E., et al. 2006, *ApJ*, 649, 759
- Clemens, D. P. 1985, *ApJ*, 295, 422
- de Wit, W. J., Testi, L., Palla, F., & Zinnecker, H. 2005, *A&A*, 437, 247
- de Wit, W. J., Hoare, M. G., Fujiyoshi, T., et al. 2009, *A&A*, 494, 157
- Di Francesco, J., Johnstone, D., Kirk, H., MacKenzie, T., & Ledwosinska, E. 2008, *ApJS*, 175, 277
- Gutermuth, R. A., Megeath, S. T., Myers, P. C., et al. 2009, *ApJS*, 184, 18
- Helfand, D. J., Becker, R. H., White, R. L., Fallon, A., & Tuttle, S. 2006, *AJ*, 131, 2525
- Jackson, J. M., et al. 2006, *ApJS*, 163, 145
- Jackson, J. M., Finn, S. C., Chambers, E. T., Rathborne, J. M., & Simon, R. 2010, *ApJ*, 719, L185
- Kirk, H., & Myers, P. C. 2011, *ApJ*, 727, 64
- Kroupa, P. 2001, *MNRAS*, 322, 231
- Lada, C. J., & Lada, E. A. 2003, *ARA&A*, 41, 57
- Lockman, F. J. 1989, *ApJS*, 71, 469

- Lucas, P. W., Hoare, M. G., Longmore, A., et al. 2008, MNRAS, 391, 136
- Maia, F. F. S., Corradi, W. J. B., & Santos, J. F. C., Jr. 2010, MNRAS, 407, 1875
- Marigo, P., Girardi, L., Bressan, A., et al. 2008, A&A, 482, 883
- Martins, F., Schaerer, D., & Hillier, D. J. 2005, A&A, 436, 1049
- Mottram, J. C., Hoare, M. G., Lumsden, S. L., et al. 2007, A&A, 476, 1019
- Ossenkopf, V., & Henning, T. 1994, A&A, 291, 943
- Rathborne, J. M., Jackson, J. M., & Simon, R. 2006, ApJ, 641, 389
- Rosolowsky, E., Dunham, M. K., Ginsburg, A., et al. 2010, ApJS, 188, 123
- Sánchez-Monge, Á., Palau, A., Estalella, R., Beltrán, M. T., & Girart, J. M. 2008, A&A, 485, 497
- Siess, L., Dufour, E., & Forestini, M. 2000, A&A, 358, 593
- Skrutskie, M. F., Cutri, R. M., Stiening, R., et al. 2006, AJ, 131, 1163
- Testi, L., Palla, F., Prusti, T., Natta, A., & Maltagliati, S. 1997, A&A, 320, 159
- Testi, L., Palla, F., & Natta, A. 1999, A&A, 342, 515
- Urquhart, J. S., Moore, T. J. T., Hoare, M. G., et al. 2011, MNRAS, 410, 1237
- White, R. L., Becker, R. H., & Helfand, D. J. 2005, AJ, 130, 586
- Weidner, C., Kroupa, P., & Bonnell, I. A. D. 2010, MNRAS, 401, 275

Table 1. Candidate UCECs

ID	l °	b °	r_c "	N_*	V_{LSR} km s ⁻¹	D kpc	M_{gas} M_\odot	R_p pc	RMS ID	Radio Continuum
(1)	(2)	(3)	(4)	(5)	(6)	(7)	(8)	(9)	(10)	(11)
1	18.3706	-0.3825	8	10	43.9	3.7	187	0.14	G018.3706-00.3818	no
2	21.2372	0.1940	9	6	25.7	2.2	65	0.10	...	no
3	24.6346	-0.3236	6	4	42.7	3.2	141	0.10	G024.6343-00.3233	no
4	28.8621	0.0653	6	3	102.8	6.8	3770	0.20	G028.8621+00.0657	maybe
5	30.4108	-0.2283	7	10	103.9	7.3	<130	0.25	G030.4117-00.2277	maybe
6	30.8191	0.2730	7	3	97.7	6.6	164	0.22	G030.8185+00.2729	maybe
7	34.7120	-0.5952	6	3	44.4	2.9	166	0.08	G034.7123-00.5946	no
8	38.9369	-0.4588	7	8	40.7	2.7	73 ^a	0.09	G038.9365-00.4592	no
9	39.4946	-0.9939	9	7	53.6	3.8	...	0.17	G039.4943-00.9933	no
10	40.3062	-0.4313	6	7	74.3	5.8	176	0.17	...	no
11	42.0981	0.3515	5	9	23.0	1.6	10	0.04	...	yes
12	43.9954	-0.0121	7	4	65.4	5.3	333	0.18	G043.9956-00.0111	no
13	50.2212	-0.6068	9	6	39.3	3.0	217 ^b	0.13	G050.2213-00.6063	no
14	52.9193	-0.8608	6	2	56.0	5.1	...	0.15	...	no
15	52.9216	-0.4889	7	5	45.0	4.2	85	0.14	G052.9221-00.4892	no
16	53.1410	0.0697	10	5	21.6	1.8	124 ^a	0.09	G053.1417+00.0705	no
17	53.2194	0.0485	10	4	23.9	1.9	17 ^a	0.09	...	no
18	59.3601	-0.2061	11	6	...	2.3 ^c	208 ^c	0.15	...	no

^aRathborne et al. (2006)

^bCalculated in Section 3.4.

^cBillot et al. (2010)

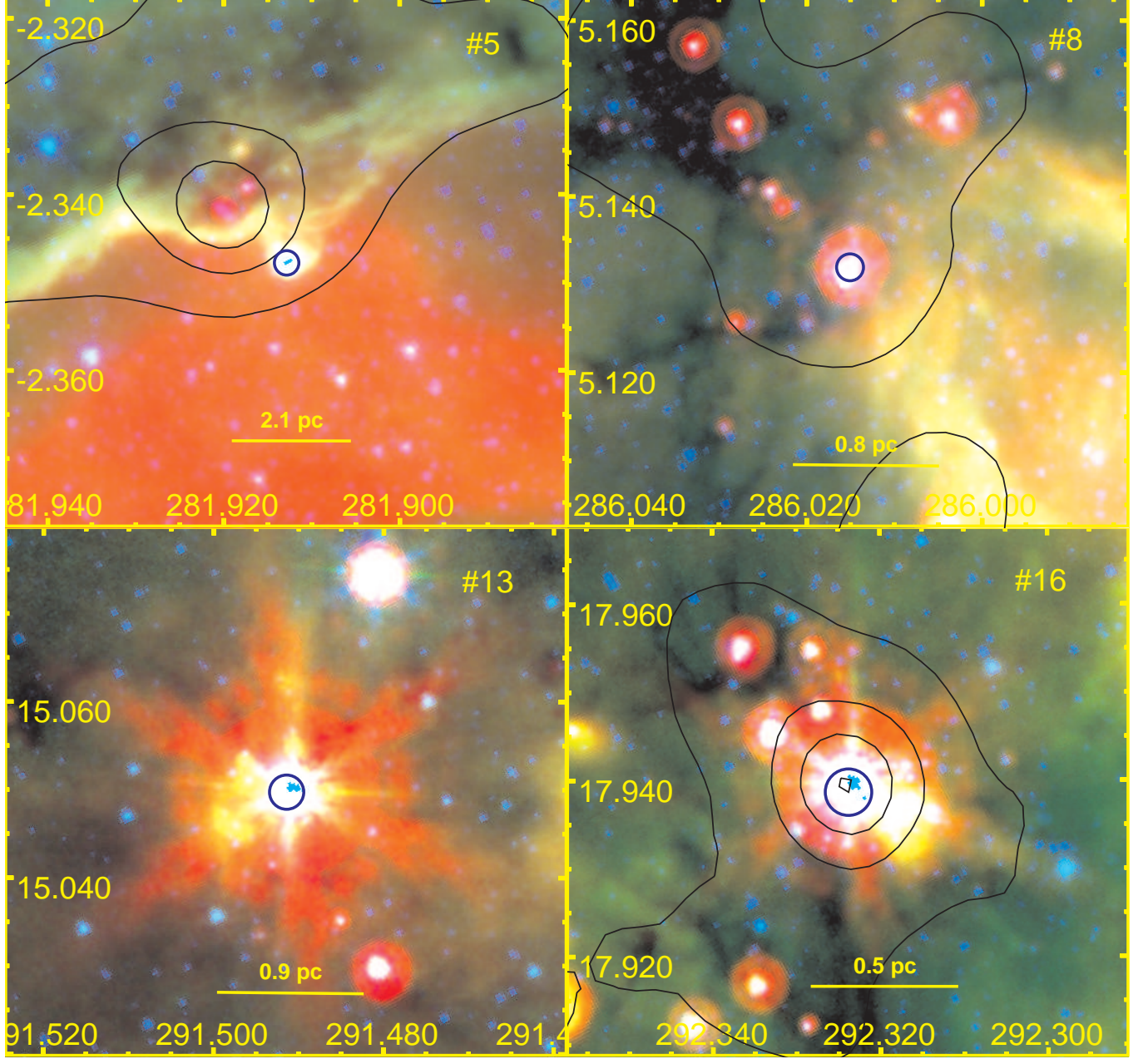


Fig. 1.— Three-color [4.5], [8.0] and [24] (blue, green, red) image of four UCECs from Table 1. They are #5 (upper left), #8 (upper right), #13 (lower left), and #16 (lower right). Blue circles indicate UCEC radii from Table 1 and the 1' yellow bar gives the linear scale at the adopted distance. Black contours outline BGPS 1.1 mm emission at 0.1, 0.6, 1.1, 1.6, and 2.1 Jy beam⁻¹. The coordinates are Equatorial J2000.

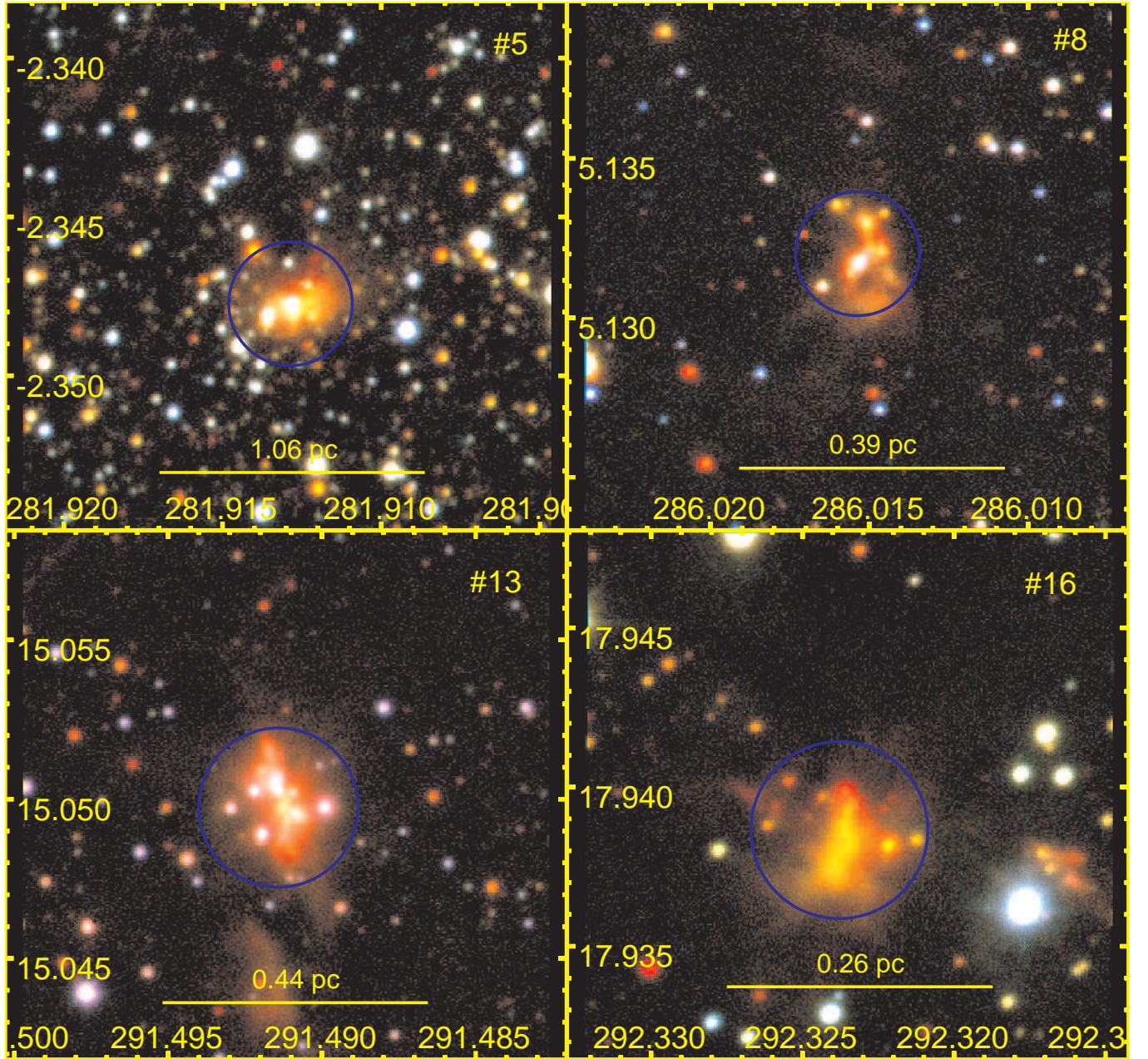


Fig. 2.— Three-color JHK (blue, green, red) image of the UCECs from Figure 1. Blue circles indicate the cluster apertures. The 30'' yellow bar shows linear scale.

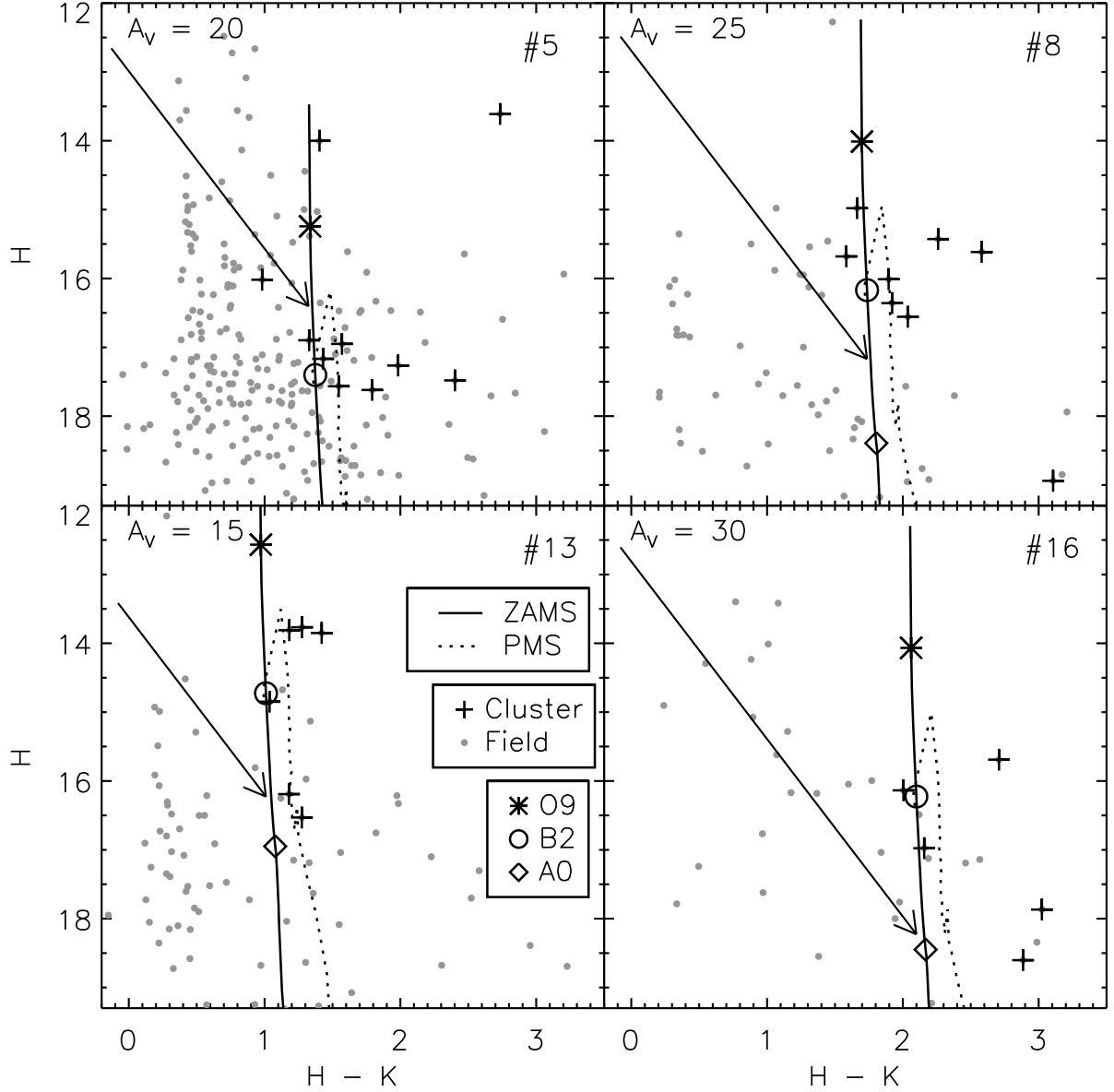


Fig. 3.— CMDs for the UCECs from Figure 1. Dots represent stars within the field annulus, between r_C and $33''$, and pluses mark sources within the cluster aperture that survive the field star subtraction ($>75\%$ probability). The solid and dotted lines are ZAMS and 0.5 Myr PMS isochrones at the cluster distance and extinguished according to the reddening vector.